Contrasting the Group 6 metal-metal bonding in sodium dichromate(II) and sodium dimolybdate(II) polymethyl complexes: Synthetic, X-ray Crystallographic and Theoretical Studies

Ross Campbell,[a] Alan R. Kennedy,[a] Ross McLellan,[a] Stuart D. Robertson,[a] Stephen Sproules[b] and Robert E. Mulvey*[a]

[a] WestCHEM, Department of Pure and Applied Chemistry, University of Strathclyde, Glasgow, G1 1XL, UK.

[b] WestCHEM, School of Chemistry, University of Glasgow, Glasgow, G12 8QQ, UK.

Email: r.e.mulvey@strath.ac.uk

Dedicated to the late Professor Malcolm Chisholm, a pioneer in metal-metal bonding chemistry

Abstract

Extending the class of group 6 metal-metal bonded methylate compounds supported by alkali metal counter-ions, the first sodium octamethylmolybdate(II) complex $[(TMEDA)Na]_4Mo_2Me_8$ and heptamethylchromate(II) relations $[(donor)Na]_3Cr_2Me_7$ (donor is TMEDA or TMCDA) are reported. The former was made by treating $[(Et_2O)Li]_4Mo_2Me_8$ with four equivalents of NaO*t*Bu/TMEDA in ether; whereas the latter resulted from introducing TMEDA or TMCDA to ether solutions of octamethyldichromate $[(Et_2O)Na]_4Cr_2Me_8$. X-ray crystallography revealed $[(TMEDA)Na]_4Mo_2Me_8$ is dimeric with square pyramidal Mo centres [including a short Mo–Mo interaction of 2.1403(3) Å] each with four methyl groups in a mutually eclipsed

conformation. In dinuclear [(TMCDA)Na]$_3$Cr$_2$Me$_7$ trigonal bi-pyramidal Cr centres each bond to three terminal methyl groups and one common Me bridge, that produces a strikingly short Cr–Cr contact of 1.9136(4) Å. Broken symmetry density functional theoretical calculations expose the multiconfigurational metal-metal bonding in these compounds with a Mo–Mo bond order of 3 computed for octamethylmolybdate(II). This is contrasted by the single Cr–Cr bond in heptamethylchromate(II) where the singlet ground state is derived by strong antiferromagnetic coupling between adjacent metal ions.

Introduction

Metal-metal bonding has been an enduring area of special interest to both synthetic and theoretical chemists. Recent achievements, such as the first crystallographic characterisations of Mg–Mg[1] and Zn–Zn[2] bonds, as well as the first isolation of a stable quintuple metal–metal bond[3] and subsequent probing of its chemistry,[4] demonstrate that this remains a topic that captures the imagination of researchers across the disciplines. Group VI metals have played a pivotal role in developing our understanding of the nature of metal–metal multiple bonding.[5] The first series of homologous metal–metal bond containing compounds belonged to this triad, specifically (COT)$_3$M$_2$ (COT = cyclooctatetraene, C$_8$H$_8$; M = Cr, Mo, W).[6] Another such early series relevant to this work was the tetralithium octamethylates Li$_4$M$_2$Me$_8$ (M = Cr, **1**; Mo, **2**),[7] novel members of the ever growing class of alkali metal ate compounds.[8] While the metal–metal bonding interactions in the Mo and W compounds are assumed to be strong, the relevance of the Cr–Cr interaction to the stability of the octamethyl complex Li$_4$Cr$_2$Me$_8$ has been cast into doubt. Evidence comes from Gambarotta's demonstration that the popular chelating

diamine TMEDA (*N*,*N*,*N'*,*N'*-tetramethylethylenediamine) can cleave the Cr–Cr "quadruple bond" in $Li_4Cr_2Me_8$ to give the mononuclear complex (TMEDA)Li(μ-Me)$_2$Cr(μ-Me)$_2$Li(TMEDA) (**3**),[9] which adopts the common Weiss motif.[10] This observation was used as evidence to suggest that the Cr–Cr close contact was in fact a forced artefact of the ligand system and that the cluster integrity was in reality sustained through a series of Li–Me–Li bridges. Recently we confirmed this assertion through the synthesis of the sodium congener $[(Et_2O)Na]_4Cr_2Me_8$ (**4**), revealing that the larger sodium cations, relative to lithium, resulted in the elongation of the Me–AM–Me (AM = Li, Na) contacts and the subsequent pronounced expansion of the Cr–Cr separation from 1.968(2) Å to 3.263(2) Å.[11] The paramagnetic nature of the sodium complex confirms the disruption of any Cr–Cr quadruple bond. Now in this paper we report the synthesis of the first sodium octamethylmolybdenum complex $[(TMEDA)Na]_4Mo_2Me_8$ (**5**) and present a clear contrast between the relative strengths of Cr–Cr and Mo–Mo interactions. Moreover we report a donor-induced, nuclearity-changing transformation of the octamethyldichromate $[(Et_2O)Na]_4Cr_2Me_8$ to the novel heptamethyldichromate $[(TMEDA)Na]_3Cr_2Me_7$ (**6**) through the *formal* elimination of one unit of MeNa. The experimental observations are evaluated with the aid of broken symmetry (BS) DFT calculations that highlight the multiconfigurational nature of the intrametal bonding in the new complexes **5** and **6**, and for contrast in **4**.

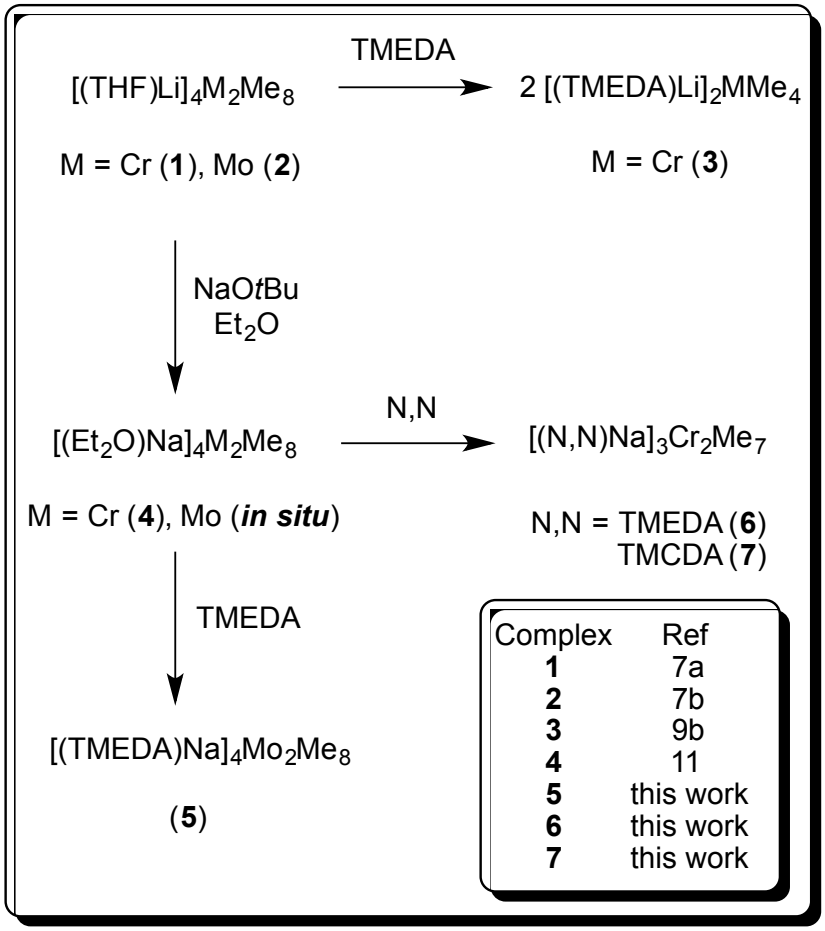

Scheme 1. Synthetic interconversions of alkali-metal group 6 methylate complexes.

Synthetic and X-ray Crystallographic Studies

Using a simple metathetical methodology, the molybdenum octamethylate $[(TMEDA)Na]_4Mo_2Me_8$ (**5**) was synthesised from the reaction of $Li_4Mo_2Me_8$ (**2**) with four molar equivalents of NaO*t*Bu/TMEDA in diethyl ether solution, furnishing a crop of red-purple crystals in a 35% yield (see Figure 1 for molecular structure). Analogous to that of $[(THF)Li]_4Mo_2Me_8$ (**2**), the sodium molybdate's core consists of two Mo centres in a square pyramidal configuration (including the Mo–Mo interaction) each with four methyl ligands in a mutually eclipsed conformation. The four [(TMEDA)Na] cations cap

the bridging faces produced by the methyl ligands, occupying sites equidistant from both Mo centres. The Mo–Mo separation in **5** is 2.1403(3) Å, which is identical within experimental error to that of the lithium congener $[(THF)Li]_4Mo_2Me_8$ (**2**) [2.148(2) Å].[7b] A key difference is that to accommodate the larger sodium cations in **5**, the alkali metals have been expelled from the core of the complex by 0.46 Å relative to the lithium compound **2**. These results confirm the intrinsic strength of the Mo–Mo quadruple bond while, at the same time, eliminating any inherent property of the octamethyl ligand set as being responsible for the significant elongation of the Cr–Cr separation within the sodium chromate $[(Et_2O)Na]_4Cr_2Me_8$ (**4**) when compared with the lithium species $[(THF)Li]_4Cr_2Me_8$ **1**. It is also noteworthy that the sodium octamethylmolybdate core remained intact even when the alkali metals are coordinated by a bidentate (TMEDA) Lewis donor.

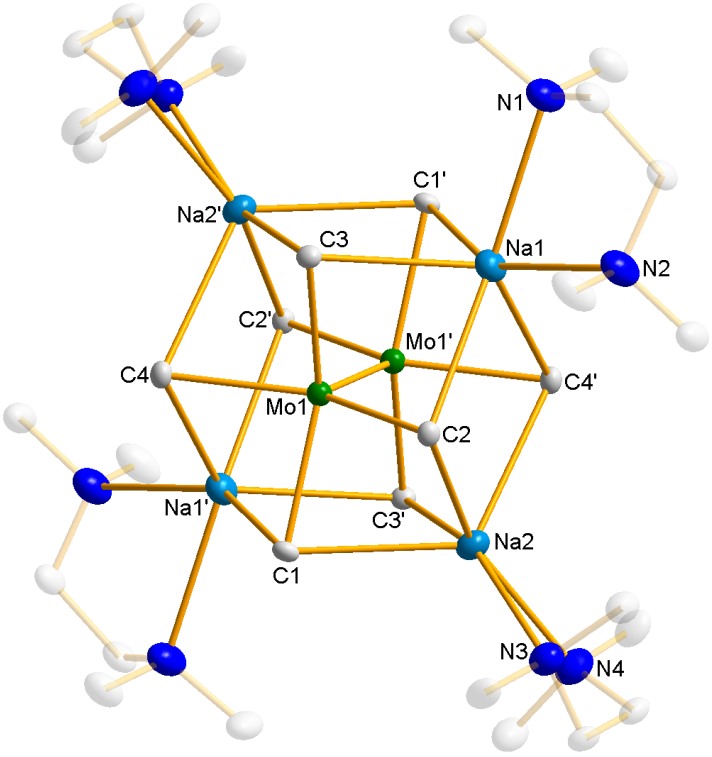

Figure 1. Molecular structure of $[(TMEDA)Na]_4Mo_2Me_8$ (**5**) with hydrogen atoms omitted for clarity. Thermal ellipsoids are represented at 50% probability. Symmetry transformation to generate atoms labeled ‘: 2-x, -y, 2-z. Selected bond lengths (Å) and angles (°): Mo1-Mo1’, 2.1403(3); Mo1-C1, 2.318(2); Mo1-C2, 2.305(2); Mo1-C3, 2.318(2); Mo1-C4, 2.324(2); Na1-C1’, 2.748(2); Na1-C2, 2.730(2); Na1-C3, 2.671(2); Na1-C4’, 2.762(2); Na1-N1, 2.614(2); Na1-N2, 2.613(2); Na2-C1, 2.731(2); Na2-C2, 2.721(2); Na2-C3’, 2.775(2); Na2-C4’, 2.756(2); Na2-N3, 2.609(2); Na2-N4, 2.605(2); C1-Mo1-Mo1’, 107.45(6); C2-Mo1-Mo1’, 107.38(5); C3-Mo1-Mo1’, 107.01(6); C4-Mo1-Mo1’, 107.62(6); C1-Mo1-C2, 84.74(8); C1-Mo1-C3, 145.52(8); C1-Mo1-C4, 84.68(8); C2-Mo1-C3, 83.93(8); C2-Mo1-C4, 144.99(8); C3-Mo1-C4, 86.20(8); Na1’-C1-Na2, 99.30(7); Na1’-C1-Mo1, 76.46(6); Na2-C1-Mo1, 76.40(6); Na1-C2-Na2, 100.41(7); Na1-C2-Mo1, 76.59(6); Na2-C2-Mo1, 76.82(6); Na1-C3-Na2’, 100.12(7); Na1-C3-Mo1, 77.62(6); Na2’-C3-Mo1, 75.78(6); Na1’-C4-Na2’, 98.77(8); Na1’-C4-Mo1, 76.10(6); Na2’-C4-Mo1, 76.08(6); N1-Na1-N2, 70.88(6); N1-Na1-C1’, 87.38(6); N1-Na1-C2, 149.84(7); N1-Na1-C3, 102.20(6); N1-Na1-C4’, 126.51(7); N2-Na1-C1’, 149.86(6); N2-Na1-C2, 88.94(6); N2-Na1-C3, 123.22(6); N2-Na1-C4’, 106.92(6); C1’-Na1-C2, 118.50(6); C1’-Na1-C3, 80.83(7); C1’-Na1-C4’, 69.14(7); C2-Na1-C3, 69.81(7); C2-Na1-C4’, 80.05(7); C3-Na1-C4’, 119.29(6); N3-Na2-N4, 71.22(6); N3-Na2-C1, 105.13(6); N3-Na2-C2, 86.96(6); N3-Na2-C3’, 153.79(6); N3-Na2-C4’, 125.41(6); N4-Na2-C1, 127.81(6); N4-Na2-C2, 154.51(6); N4-Na2-C3’, 85.55(6); N4-Na2-C4’, 101.31(6); C1-Na2-C2, 69.71(6); C1-Na2-C3’, 79.31(7); C1-Na2-C4’, 118.98(6); C2-Na2-C3’, 118.22(6); C2-Na2-C4’, 80.33(7); C3’-Na2-C4’, 69.98(7).

We next set out to build upon Gambarotta's earlier work by further expanding the family of TMEDA solvated group VI methylate complexes to include a TMEDA solvated sodium chromate. Thus, taking a pre-prepared ether solution of the sodium chromate $[(Et_2O)Na]_4Cr_2Me_8$ (**4**) and introducing four molar equivalents of the diamine TMEDA at -30 °C gave a red/brown solution. A crop of intensely dark red crystals was then produced on storage of the solution at -70 °C. Single crystal X-ray diffraction analysis (Figure 2) gave a surprising result in revealing the product to be an unprecedented heptamethyl dichromate $[(TMEDA)Na]_3Cr_2Me_7$ (**6**), formed through the formal loss of a MeNa(TMEDA) fragment. The generality of this reaction was confirmed by a reaction using the bidentate donor *N*,*N*,*N*′,*N*′-tetramethylcyclohexanediamine (TMCDA) which yielded the analogous TMCDA complex $[(TMCDA)Na]_3Cr_2Me_7$ (**7**, Figure 2). As the two complexes are isostructural, the discussion of the crystallographic data will be limited to **7**, which did not display any donor disorder and was of a higher quality than that of **6**.

Each Cr centre within **7** adopts a distorted trigonal bi-pyramidal geometry with the other Cr fulfilling the role of one of the equatorial constituents. Two methyl ligands occupy the remaining equatorial sites with a further two methyl ligands in axial positions, one of which (C7) now acts as a bridge between the two Cr centres, allowing each metal to maintain coordination to four methyl anions. The Cr to bridging methyl ligand bond distances are the longest in the complex with an average $Cr–Me_{bridge}$ bond length of 2.294 Å compared with an average $Cr–Me_{terminal}$ bond distance of 2.171 Å. The Cr-Me-Cr unit is noticeably different than the corresponding fragment seen in Power's Cr(II) complex $[ArCr(\mu\text{-}Me)]_2$ [Ar = C_6H-2,6-(C_6H_2-2,4,6-*i*Pr_3)$_2$-3,5-*i*Pr_2],[12] with a more acute Cr-C-Cr

angle [49.30(5)^{o} versus 75.75^{o}) and consequently a shorter Cr···Cr separation [1.9136(4) Å, *vide infra*, versus 2.6941(5) Å] seen in **7**. This difference may be attributed to the close proximity of flanking substituted aryl groups of the terminal polyaromatic ligand in Power's complex, which may have the steric effect of 'pushing' the bridging methyl groups closer together, hence widening the angle at C and concomitantly lengthening the metal-metal separation, whereas the bridging methyl in **7** is relatively unencumbered. There are two distinct sodium environments, with those of Na(2) and Na(3) replicating that seen in previous M_2Me_8 complexes, namely acting as a cap to four methyl anions. However, the formal absence of the eighth methyl group, and the subsequent slippage of C7 from a terminal to a bridging environment, leaves Na(1) capping only three methyl groups. The asymmetry of the complex, with respect to alkali metal octamethylchromates such as **1** and **4**, is reflected in the distinct Na-methyl bond distances observed. Those sodiums centres which cap four methyl groups (Na2 and Na3) display an average Na-C distance of 2.806 and 2.819 Å respectively while Na1, which caps only three methyl groups, has an average distance of 2.601 Å. The formally vacant site (that is formed by the 'absence' of one MeNa unit) allows Na2 to migrate slightly in that direction, with the distances to C5 and C6 [2.631(3)/2.786(3) Å] being noticeably shorter than to C3 and C4 [2.814(2)/2.993(2) Å]. However, the most striking feature of **7** is the short Cr–Cr contact of 1.9136(4) Å, which is comparable to that in Krausse's original lithium chromate species $[(THF)Li]_4Cr_2Me_8$ [**1**, 1.968(2) Å].[7a]

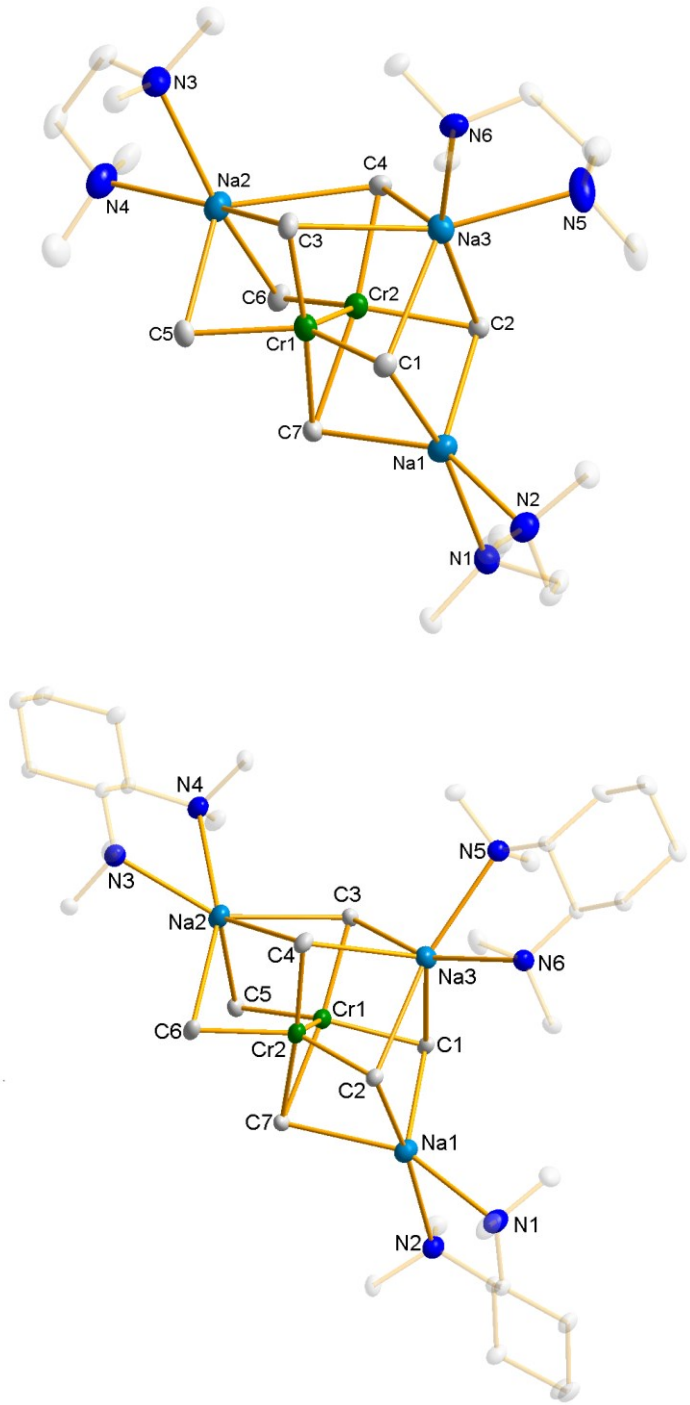

Figure 2. Molecular structure of $[(TMEDA)Na]_3Cr_2Me_7$ (**6**, top) and $[(TMCDA)Na]_3Cr_2Me_7$ (**7**, bottom) with hydrogen atoms and minor disorder of one TMEDA ligand of **6** omitted for clarity. Thermal ellipsoids are represented at 50% probability.

	6	**7**		**6**	**7**		**6**	**7**
Cr1-Cr2	1.9270(9)	1.9136(4)	Na3-C3	2.796(5)	2.759(2)	C6-Cr2-C7	87.5(2)	88.17(9)
Cr1-C1	2.194(4)	2.205(2)	Na3-C4	2.673(5)	2.769(2)	C6-Cr2-Cr1	112.21(17)	112.67(7)
Cr1-C3	2.159(5)	2.160(2)	Na3-N5	2.581(7)	2.609(2)	C7-Cr2-Cr1	64.8(2)	65.77(6)
Cr1-C5	2.154(4)	2.160(2)	Na3-N6	2.580(7)	2.607(2)	Na1-C1-Na3	99.13(16)	96.93(7)
Cr1-C7	2.287(7)	2.302(2)				Na1-C1-Cr1	85.44(18)	87.75(7)
Cr2-C2	2.181(5)	2.174(2)	C1-Cr1-C3	88.8(2)	87.49(8)	Na3-C1-Cr1	73.17(14)	73.11(6)
Cr2-C4	2.169(5)	2.185(2)	C1-Cr1-C5	134.34(19)	134.02(9)	Na1-C2-Na3	95.67(16)	93.78(7)
Cr2-C6	2.153(5)	2.142(2)	C1-Cr1-C7	99.8(2)	98.82(8)	Na1-C2-Cr2	86.38(17)	88.79(8)
Cr2-C7	2.302(7)	2.286(2)	C1-Cr1-Cr2	111.03(13)	113.12(6)	Na3-C2-Cr2	70.46(13)	72.02(6)
Na1-C1	2.540(6)	2.544(2)	C3-Cr1-C5	88.0(2)	91.23(9)	Na2-C3-Na3	102.79(16)	105.88(8)
Na1-C2	2.562(6)	2.634(2)	C3-Cr1-C7	171.3(2)	173.27(9)	Na2-C3-Cr1	69.94(14)	73.07(6)
Na1-C7	2.544(6)	2.625(2)	C3-Cr1-Cr2	112.43(14)	110.50(7)	Na3-C3-Cr1	74.25(14)	75.73(7)
Na1-N1	2.480(4)	2.512(2)	C5-Cr1-C7	85.3(2)	86.05(9)	Na2-C4-Na3	102.37(17)	100.97(8)
Na1-N2	2.584(4)	2.544(2)	C5-Cr1-Cr2	112.21(17)	110.27(7)	Na2-C4-Cr2	68.05(13)	71.06(7)
Na2-C3	2.932(5)	2.814(2)	C7-Cr1-Cr2	65.6(2)	64.93(7)	Na3-C4-Cr2	76.37(15)	74.67(6)
Na2-C4	3.063(5)	2.993(2)	C2-Cr2-C4	89.7(2)	90.20(9)	Na2-C5-Cr1	77.79(15)	77.06(8)
Na2-C5	2.572(6)	2.631(3)	C2-Cr2-C6	132.4(2)	131.62(9)	Na2-C6-Cr2	78.54(16)	76.11(7)
Na2-C6	2.588(6)	2.786(3)	C2-Cr2-C7	97.0(2)	95.16(8)	Na1-C7-Cr1	83.46(19)	83.85(7)
Na2-N3	2.538(4)	2.558(2)	C2-Cr2-Cr1	112.48(13)	112.56(6)	Na1-C7-Cr2	84.34(19)	86.69(8)
Na2-N4	2.574(4)	2.663(2)	C4-Cr2-C6	88.8(2)	88.26(10)	Cr1-C7-Cr2	49.66(12)	49.30(5)
Na3-C1	2.824(5)	2.851(3)	C4-Cr2-C7	173.2(2)	174.64(8)			
Na3-C2	2.942(5)	2.899(2)	C4-Cr2-Cr1	111.54(16)	112.11(7)			

Table 1 Selected bond parameters (Å/^{o}) of complexes **6** and **7**.

Comparing the reactivities of the lithium and sodium octamethyldichromates $[M]_4Cr_2Me_8$ [M = (THF)Li (**1**); (Et_2O)Na, (**4**)] towards the Lewis base TMEDA provides another remarkable example of the important role alkali metals can play in dictating structural motifs within chromium species. While Gambarotta has demonstrated the symmetrical cleavage of the lithium species to give the mononuclear compound $[(TMEDA)Li]_2CrMe_4$ (**3**),[9b] the sodium congener has instead favoured the formal elimination of a unit of (TMEDA)NaMe to provide the dinuclear heptamethyldichromate **6** (scheme 2). Examining the transformation from the octamethyl complex $[(THF)Na]_4Cr_2Me_8$ to the TMEDA solvate **6** also reveals the significant potential provided by the subtleties of Cr(II) metal–metal bonding; the ability to profoundly alter the electronic and magnetic properties at the metal centre by the seemingly simple switching of the peripheral Lewis base. Dinuclear group VI metal species, including those of Cr, have already been demonstrated as useful catalysts.[13] Indeed dinuclear Cr species have recently been implicated in the commercially highly significant selective tetramerisation of ethylene to 1-octene.[14] One can envisage how sophisticated Cr based complexes could be designed in the future, taking advantage of the inherent lability of the Cr–Cr bond, to produce highly tuneable, potentially substrate selective catalysis.

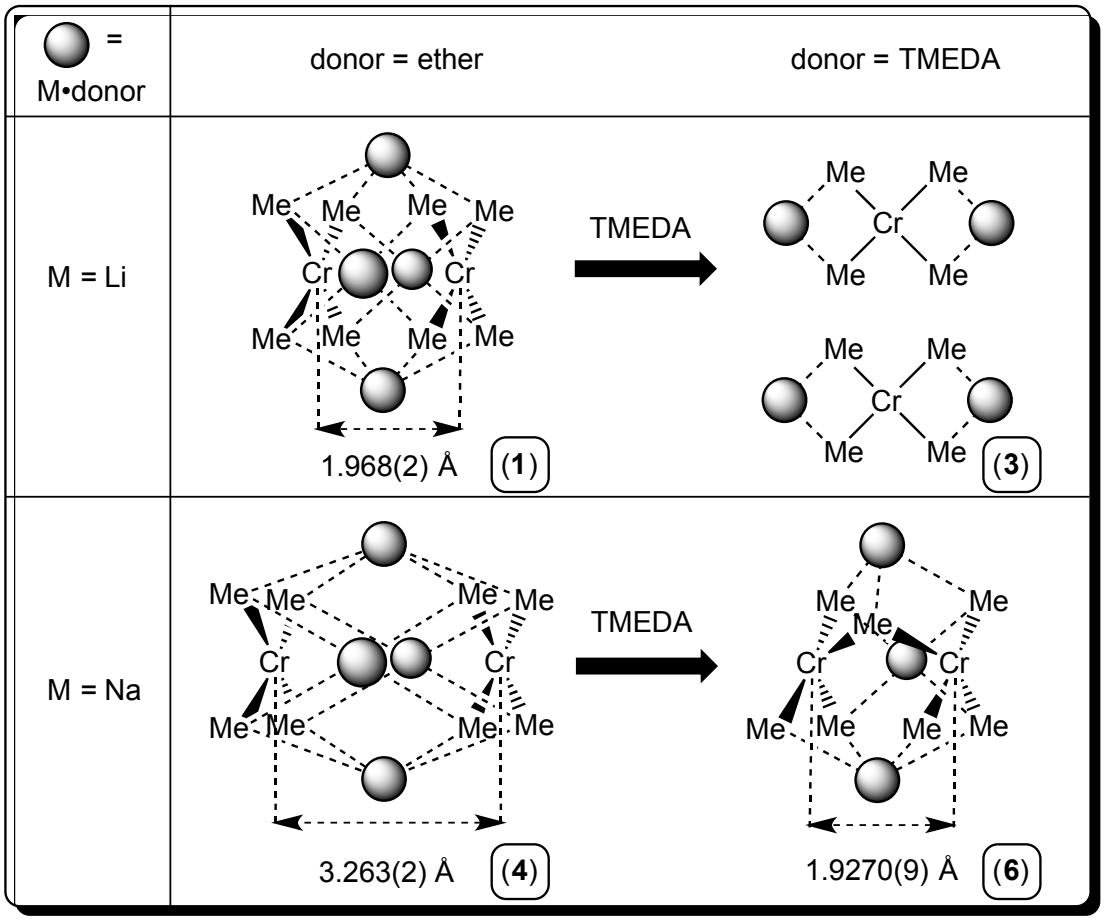

Scheme 2. Highlighting the reactivity contrast of the lithium and sodium octamethyldichromate complexes towards the diamine TMEDA.

In solution, **5** displays clean ^{1}H and ^{13}C NMR spectra confirming metal coordination of the TMEDA ligand, while the metal bound methyl groups resonate at -1.11 and 3.0 ppm respectively, consistent with close proximity to electropositive metals. **6** and **7** gave far broader spectra, consistent with paramagnetic species. Indeed, the methyl resonances in **7** were too broad to be discernible in either spectra while **6** only gave a very broad resonance in the ^{1}H NMR spectrum (-0.24 ppm), again due to the effect of nearby metal centres.

Calculations

The electronic structure and description of the intrametal bonding in **4**, **5** and **6** is derived from broken symmetry (BS) DFT calculations using the BP86 functional for geometry optimisations and the PBE0 functional for electronic properties. Although these compounds are anions, the inclusion of Na^+ counter-ions in their cage-like structure ensured the solvent continuum had no effect on the computed geometry or electronic structure. The calculated geometries and metrical parameters of **5** and **6** were found to be in excellent agreement with those determined experimentally (Tables S1 and S2), though this is not surprising given the rigidity of these structures and the propensity of group 6 elements to form metal-metal bonds.[15] For **5** (Figure S1), the optimised Mo–Mo and average Mo–C bond lengths are very slightly underestimated by 0.003 Å and 0.006 Å, respectively. The average Na–C bond distance shows a larger departure from the solid state structure by 0.02 Å, and the Na–N distances are on the whole 0.04 Å shorter in the optimized structure. These peripheral components have no impact on the intrinsic electronic structure of these compounds. Interestingly, the dichromium analogue, **4**, failed to converge, underscoring the dominant role of the Na^+ ions in maintaining the long Cr···Cr distance seen experimentally.[11]

In a simple ligand field description, the available d orbitals for each metal ion in **5** form metal-metal bonds:[15] one σ bond between d_{z^2} orbitals; two π bonds between d_{xz} and d_{yz} orbitals, and a δ bond between d_{xy} orbitals, where the *z*-axis is parallel to the metal-metal vector. The $d_{x^2-y^2}$ orbital is preoccupied by the strongly σ-donating Me ligands. Given the inherently multiconfigurational nature of metal-metal bonds, the electronic structure of **5** has been investigated using broken symmetry BS(1,1) and BS(4,4) calculations. These configurations describe the number of singly-occupied orbitals (SOMO) localized to each Mo ion. For the BS(1,1) calculation, these are the

d_{xy} orbitals that constitute the δ bond and the most orthogonal pair of SOMOs. The BS(4,4) configuration calculates eight SOMOs where all four unpaired electrons are localised to the Mo(II) ions. There are no Mo–Mo bonds is this solution as the overlap of SOMOs is too small to constitute a covalent interaction. Rather, symmetry equivalent d orbitals couple and the strength of this exchange interaction is a function of the degree of their spatial overlap and evaluated by the exchange coupling constant (*J*) given by the difference in total energy of the high spin (uncoupled) and broken symmetry (coupled) solutions.[16] In addition a spin unrestricted Kohn-Sham $S = 0$ (singlet) state is calculated to contrast the broken-symmetry configurations, as this represents a quadruply bonded dimolybdenum(II) system.

For **5**, the BS(1,1) $S = 0$ solution is the most favourable, by 7.1 kcal mol^{-1} over the UKS singlet solution, and 11.6 kcal mol^{-1} over the triplet ($S = 1$) solution. The BS(4,4) calculation converged to the same solution as the BS(1,1), commensurate with the multiconfigurational character of the metal-metal bond. Also the Mo–Mo distance of 2.1403(3) Å in **5**, and similarly long bond in the Li analogue (**2**) of 2.148(2) Å,[7b] are on the high end in Mo–Mo quadruply bonded complexes.[17] The MO manifold calculated for **5** is shown in Figure 3, and reveals two Mo(II) d^4 ions forming one σ bond and two π bonds. The strength of the Me ligands imposes an antibonding interaction with the Mo_2 σ-type orbital that destabilises it above the π-type MOs, as encountered with other strong field ligand systems.[18] The strong ligand field is likely responsible for the absence of the Mo–Mo δ-bond between neighbouring d_{xy} orbitals, as this orbital projected into the plane of four Me ligands. Instead, these magnetic orbitals couple antiferromagnetically with each other to give the singlet ground state. An orbital overlap integral S = 0.54 is computed for **5**, and represents the extent of spatial overlap of the two SOMOs.[19] A value of S = 0

indicates the two magnetic orbitals are orthogonal, whereas S = 1 implies a doubly occupied orbital (DOMO) – a covalent bond. The exchange coupling constant, determined from the high spin and BS energies together with the corresponding spin-expectation values according to the Yamaguchi approach (Eq. 1),[16] is calculated to be -3282 cm^{-1}, in keeping with the observed singlet ground state of the molecule. The Mulliken spin density analysis shows +1.46 (α-spin) on one Mo ion and the corresponding amount of -1.46 (β-spin) on the other (Figure 4a). This value is markedly higher than one as a result of the polarised Mo–Mo bond as well as polarised Mo–C σ-bonds that deposits 0.22 spins over the four Me ligands bound to each Mo ion.

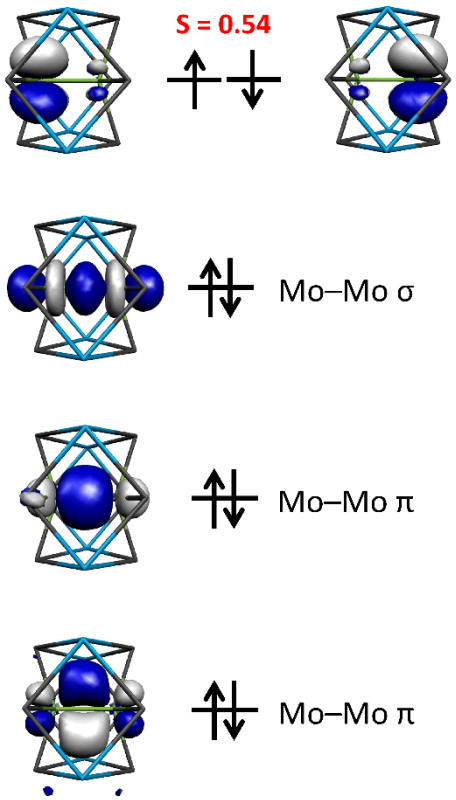

Figure 3. Qualitative MO scheme depicting the ordering of the frontier Mo d orbitals for **5** showing three Mo–Mo bonds and one pair of corresponding MOs that constitute the BS(1,1) *S* = 0 solution. The S-value indicates the calculated overlap between

corresponding orbitals. Hydrogen atoms and TMEDA solvent molecules have been omitted for clarity.

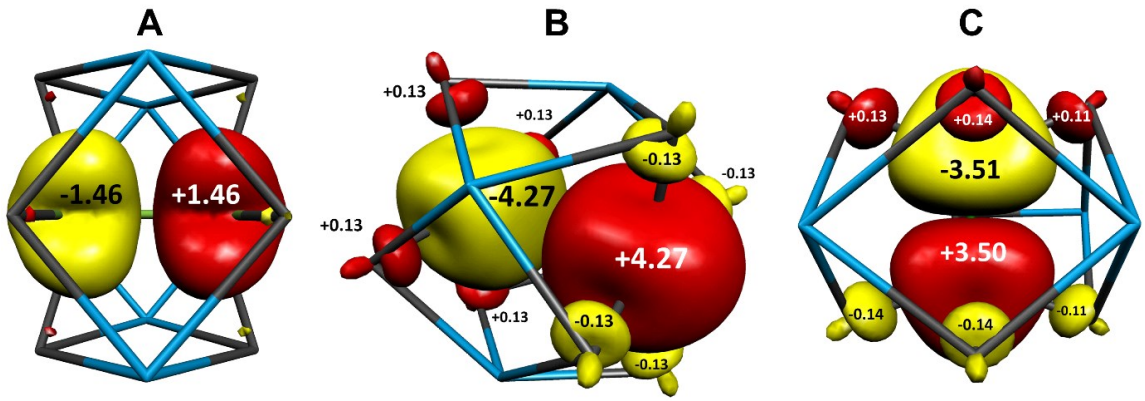

Figure 4. Spin density plots from Mulliken spin population analyses. (a) **5**, (b) **4**, (c) **6** (red: α-spin; yellow: β-spin). Hydrogen atoms and solvent molecules have been omitted for clarity.

In contrast to **5**, the Cr atoms in **4** were calculated to be noninteracting and to behave as individual Cr(II) d^4 (S_{Cr} = 2) ions. Its electronic structure is defined as a BS(4,4) solution, where the S = 0 solution was 7.8 kcal mol^{-1} more stable than the high spin S = 4 solution. The spin unrestricted Kohn-Sham S = 0 (singlet) calculation failed to converge as the long intrametal distance precludes any Cr-Cr bond formation. The MO scheme shown in Figure 5 depicts eight SOMOs with >90% Cr character with symmetrically equivalent pairs coupled antiferromagnetically to each other. The large Cr···Cr gap is reflected in the very small overlap integrals (S) for corresponding pairs; the δ-interacting pair of d_{xy} orbitals are wholly orthogonal. The overlap is slightly higher for the π-interacting d orbitals, whereas a reasonably strong coupling interaction is evident for the d_{z^2} orbitals with S = 0.57. The calculated Mayer bond order of 0.16 confirms these Cr ions are not bonded to each other. This weak

interaction manifests in the calculated exchange coupling constant of J = -169 cm^{-1} as the difference in energy between the BS (S = 0) and high spin (S = 4) solutions. This miniscule value is corroborated by variable temperature magnetic susceptibility data recorded for **4** that showed population of paramagnetic states < 5 K.[11] The room temperature magnetic moment of 2.45 μ_B indicates significant population of the S = 1 and S = 2 paramagnetic exited states at the expense of the diamagnetic ground state (S = 0) in this weakly coupled system. The Mulliken spin density analysis shows +4.27 on one Cr ion and -4.27 spins on the other (Figure 4b) consists with high spin S_{Cr} = 2 metal centres. The value is slightly higher than 4 on account of the pronounced polarisation of the Cr–C σ-bonds that deposits 0.69 spins of opposing sign over the four Me ligands bound to each Cr ion.

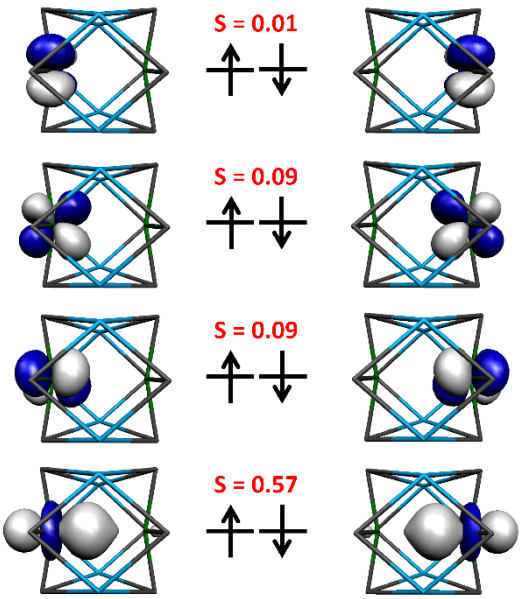

Figure 5. Broken-symmetry molecular orbital diagram for **4** with the corresponding molecular orbitals shown to the left and right that constitute the BS(4,4) S = 0 solution. The S-value indicates the calculated overlap between corresponding orbitals. Hydrogen atoms and THF solvent molecules have been omitted for clarity.

The geometry optimized structure of **6**, calculated using spin-unrestricted BS-DFT at the BP86 level, is almost identical to the solid state structure (Figure S2). The computed Cr–Cr distance of 1.858 Å is an underestimate of the experimental one at 1.9270(9) Å, with a concomitant decrease in the Cr–C(7)–Cr angle to 46.7° (Table S2). Overall, the Cr–C and Na–C distances are well reproduced, aside from a significantly lengthening of the Cr(2)–C(7) bond – this being the bridging Me ligand. There is a shortening of the average Na–N distance as seen with **4**.

The Cr–Cr interaction in **6** is highly multiconfigurational giving rise to a BS(3,3) solution for a total spin ground state of $S = 0$. This state is a colossal 65.5 kcal mol^{-1} more stable than the high spin ($S = 3$) solution, and 62.4 kcal mol^{-1} lower in energy than the spin-unrestricted Kohn-Sham singlet solution that constitutes quadruply bonded metal ions. This underscores the reluctance of Cr ions to bind with each other even at intermetal distances suggestive of multiple metal bonding. Both **6** and **7** have Cr–Cr distances even shorter than that of **1** (2.199 Å)[7a] which arise not from the formation of multiple metal bonds but rather the Cr ions are tethered by the bridging Me ligand even when the bulkier Na ions are inserted into the structure. The MO scheme presented in Figure 6 reveals a Cr–Cr σ-bond and three pairs of magnetic orbitals, one σ-type, one π-type and third a δ-type interaction. The latter shows the smallest overlap, whereas the other two give reasonably large overlap integrals that is reflected in the strong exchange coupling between the Cr(II) ions of $J = -2398$ cm^{-1}, which is also mediated by the bridging Me ligand. The stronger exchange coupling constant is commensurate with a mediocre effective magnetic moment of 1.05 μB recorded on a powder sample of **6** at room temperature. The order of magnitude larger *J*-value for **6** compared to **4** reflects the smaller thermal depopulation of the spin coupled $S = 0$ ground state at this temperature. This calculated Mayer bond order of

1.22 is consistent with this electronic structure and that despite their close proximity; the Cr ions are effectively weakly coupled and therefore easily disrupted.[9b, 11, 20] The Mulliken spin population analysis reveals 3.5 spins per Cr ion (Figure 4c). The highly polarised Cr–C bonds, a feature of metal-alkyl organometallic compounds, is ~0.4 spins on the three terminal Me ligands for each Cr centre; the bridging Me ligand carries no spin density. There is an additional polarisation of the Cr–Cr σ-bond which elevates the spin density well above the expected three in a dichromium(II) compound with a single metal-metal bond.

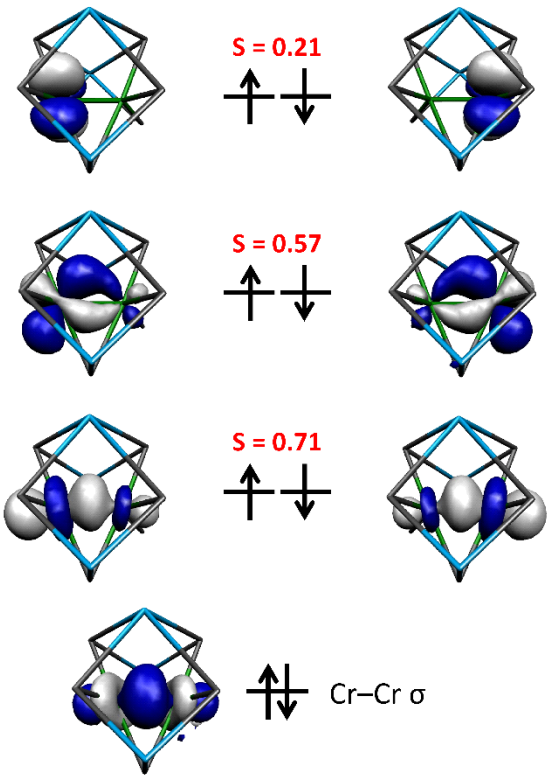

Figure 6. Broken-symmetry molecular orbital diagram for **6** with the corresponding molecular orbitals shown to the left and right. The S-value indicates the calculated overlap between corresponding orbitals. Hydrogen atoms and THF solvent molecules have been omitted for clarity.

The chemical properties of these two group 6 metals – Cr and Mo – are neatly contrasted in these dimetallic compounds. The larger, more diffuse 4d orbitals of the heavier congener provide a clear preference for Mo–Mo multiple bond character. In contrast, Cr(II) is more Lewis acidic. The 3d orbitals are more contracted and the metal-ligand bonding tending to ionic rather than covalent preferred by the 4d and 5d metals. Therein, Cr has an inherent reluctance to form multiple metal-metal bonds,[18, 21] and the weak Cr···Cr is interaction is readily disrupted. This is exemplified by the increased intermetal distance in **4** when Na^+ replaces the Li^+ from the precursor, **1** (Scheme 1). Even in the systems with a short intermetal distance, the Cr–Cr bond is weak, and best portrayed as a single or double bond with additional support from exchange coupled magnetic orbitals. It is important to point out that the DFT-derived estimates of the *J*-values for **4** of -169 cm^{-1} and **6** of -2398 cm^{-1} (*ca*. 0.5 and 6.9 kcal mol^{-1}, respectively) are significantly smaller than the energy supplied by Na^+–C bonds when the Li^+ ions are displaced. Thus, the experimentally observed Cr–Cr distances in these organometallic dimers is driven almost exclusively by the bond distances and angles preferences of the alkali metal, and assisted by the strong field Me ligands that enhance the polarisation of the metal-ligand and metal-metal bonds. Conversely, the dimolybdenum analogues will retain their robust Mo–Mo bond irrespective of additions to the second coordination and peripheral solvent coordination sphere.

Conclusion

This work has seen the synthesis and crystallographic characterisation of the sodium octamethylmolybdate complex $[(TMEDA)Na]_4Mo_2Me_8$ and demonstrated through a series of theoretical calculations that it contains a metal–metal triple bond. It has also

established that the octamethyldichromate $[(Et_2O)Na]_4Cr_2Me_8$ surprisingly decreases its nuclearity by one (formally by displacement of a donor·NaMe fragment) on addition of the stronger bidentate donors TMEDA or TMCDA to generate the novel heptamethyldichromate complexes $[(TMEDA \text{ or } TMCDA)Na]_3Cr_2Me_7$. Unlike the related dimolybdate complex, these dichromates exhibit a weaker intermetal interaction appraised as only a single Cr–Cr bond despite their small spatial separation. The tethering of the Cr(II) ions by a methyl bridge in the heptamethyldichromate complexes (**6** and **7**) exacerbates the shortness of these Cr···Cr separations, and strengthens the exchange interaction between adjacent Cr(II) ions that gives rise to the singlet ($S = 0$) spin ground state. Finally, these results with sodium in departing markedly from those of related lithium species illustrate the profound influence the choice of alkali metal can have on the structure and reactivity of these transition metal complexes.

Experimental

General Information. All reactions and manipulations were carried out in an atmosphere of dry pure argon gas using standard Schlenk and glovebox techniques. Diethyl ether was distilled from sodium benzophenone. $CrCl_2$ and NaO*t*Bu were purchased from Aldrich and used as received. $[(Et_2O)Na]_4Cr_2Me_8$ was prepared by a previously published procedure.[11] Despite several attempts, satisfactory elemental analyses of compounds **5-7** could not be obtained because of their highly air- and moisture-sensitive nature. NMR spectra were recorded on a Bruker AV400 MHz spectrometer (operating at 400.03 MHz for ^1H and 100.58 MHz for ^{13}C). All ^{13}C NMR spectra were proton decoupled. Room temperature magnetic moments were acquired using a magnetic susceptibility balance (Sherwood Scientific Mark I).

X-ray crystallography

Crystallographic data were collected on Oxford Diffraction instruments with Mo Kα radiation (λ = 0.71073 Å). Structures were solved using SHELXS-97[22] or OLEX2,[23] while refinement was carried out on F^2 against all independent reflections by the full matrix least-squares method using the SHELXL-97 program or by the GaussNewton algorithm using OLEX2. All non-hydrogen atoms were refined using anisotropic thermal parameters. Selected crystallographic details and refinement details are provided in table S3. CCDC 1519879-1519881 contains the supplementary crystallographic data for these structures. These data can be obtained free of charge from the Cambridge Crystallographic Data Centre via www.ccdc.cam.ac.uk/data_request/cif.

Calculations

The program package ORCA was used for all calculations.[24] The geometries of **5** and **6** were fully optimised by a spin unrestricted DFT method employing the BP86[25] functional with THF as solvent. The stability of all solutions was checked by performing frequency calculations: no negative frequencies were observed. Triple-ξ-quality basis sets with one set of polarization functions (def2-TZVP) were used for all atoms.[26] The single-point calculations were performed with PBE0[27] functional on optimised and crystallographic coordinates using the same basis sets and enhanced integration accuracy for metal atoms (SPECIALGRIDINTACC 10). A scalar relativistic correction was applied using the zeroth-order regular approximation (ZORA) method,[28] with dispersion effects including using the D3[29] method. The RIJCOSX approximation[30] combined with the appropriate Ahlrichs auxiliary basis set

was used to speed up the calculations.[31] The conductor like screening model (COSMO) was used for all calculations.[32] The geometry search for all complexes was carried out in redundant internal coordinates without imposing geometry constraints. The self-consistent field calculations were tightly converged (1×10^{-8} E_h in energy, 1×10^{-7} E_h in the density charge, and 1×10^{-7} in the maximum element of the DIIS[33] error vector). The geometry was converged with the following convergence criteria: change in energy $<10^{-5}$ E_h, average force $<5 \times 10^{-4}$ E_h Bohr^{-1}, and the maximum force 10^{-4} E_h Bohr^{-1}.

We used the broken symmetry (BS) approach to describe our computational results for all compounds.[34] We adopted the following notation: the given system was divided into two fragments. The notation BS(m,n) refers then to a broken symmetry state with m unpaired α-spin electrons essentially on fragment 1 and n unpaired β-spin electrons localized on fragment 2. In each case, fragments 1 and 2 correspond to the two metal ions. In this notation the standard high spin, open-shell solution is written as BS(m+n,0). The BS(m,n) notation refers to the initial guess to the wavefunction. The variational process does, however, have the freedom to converge to a solution of the form BS(m−n,0) in which effectively the n β-spin electrons pair up with $n < m$ α-spin electrons on the partner fragment. Such a solution is then a standard $M_S \approx (m-n)/2$ spin-unrestricted Kohn-Sham solution. As explained elsewhere,[19] the nature of the solution is investigated from the corresponding orbital transformation (COT) which, from the corresponding orbital overlaps, displays whether the system should be described as a spin-coupled or a closed-shell solution. The exchange coupling constants J were obtained from broken symmetry solution using Eq. 1,[16] and assuming the spin-Hamiltonian Eq. 2 is valid,

$$J = \frac{E_{HS} - E_{BS}}{\langle \hat{S}^2 \rangle_{HS} - \langle \hat{S}^2 \rangle_{BS}} \qquad (1)$$

$$\hat{H} = -2J\hat{S}_A \cdot \hat{S}_B \qquad (2)$$

where E_{BS} is the energy of the broken symmetry solution, E_{HS} is the energy of the high spin state, $\langle \hat{S}^2 \rangle_{HS}$ is the expectation value of $\hat{S}^2$ operator for the high spin state, $\langle \hat{S}^2 \rangle_{BS}$ is the expectation value of $\hat{S}^2$ operator for the broken symmetry solution, and $\langle \hat{S}^2 \rangle_{HS}$ is the expectation value of $\hat{S}_A^2$ and $\hat{S}_B^2$ are local spin operators. Molecular orbitals and spin density maps were visualised via the programme Molekel.[35]

Synthesis of [(TMEDA)Na]$_4$Mo$_2$Me$_8$ (5)

0.43 g (1 mmol) of [Mo(O$_2$CCH$_3$)$_2$]$_2$ was suspended in 30 mL of diethyl ether and cooled to 0 °C. A purple colour was produced on the dropwise introduction of MeLi [5 mL of a 1.6 M solution in diethyl ether (8 mmol)]. The resulting suspension was stirred for 18 h whilst maintaining the temperature at 0 °C before the solids were removed by filtration and washed with a further 10 mL diethyl ether. The purple solution was then re-cooled to 0 °C and 0.38 g (4 mmol) of NaO*t*Bu and 0.60 mL (4 mmol) of TMEDA were added. The resulting solution was stirred for 1 h, concentrated *in vacuo* and stored at -30°C overnight yielding a crop of red crystals (0.30 g, 35 % yield). ^{1}H NMR (400.13 MHz, THF-d_8, 300 K: δ(ppm) = 2.31 (s, 16 H, C*H*$_2$ TMEDA), 2.16 (s, 48 H, C*H*$_3$ TMEDA), -1.11 (s, 24 H, Me). ^{13}C{^{1}H} NMR (100.62 MHz, THF-d_8, 300 K): δ(ppm) = 58.9 (*C*H$_2$ TMEDA), 46.3 (*C*H$_3$ TMEDA), 3.0 (Me).

Synthesis of [(TMEDA)Na]$_3$Cr$_2$Me$_7$ (6)

0.31 g (0.5 mmol) [(Et$_2$O)Na]Cr$_2$Me$_8$ was dissolved in 20 mL diethyl ether and cooled to -30 °C. The addition of 0.30 mL (2 mmol) TMEDA produced a red brown solution which was stirred for 1 h. After concentration *in vacuo* the solution was stored at -70

°C giving intensely dark red crystals in a 48 % (0.15 g) yield. ^{1}H NMR (400.13 MHz, C_6D_6, 300 K: δ(ppm) = 2.19 (bs, 36 H, C*H*$_3$ TMEDA), 2.00 (bs, 12 H, C*H*$_2$ TMEDA), -0.24 (bs, 21 H, Me). ^{13}C{^{1}H} NMR (100.62 MHz, C_6D_6, 300 K): δ(ppm) = 57.4 (*C*H$_2$ TMEDA), 46.2 (*C*H$_3$ TMEDA). μ_{eff} (solid, Gouy balance, 25 °C) = 1.05 μ_B.

Synthesis of [(TMCDA)Na]$_3$Cr$_2$Me$_7$ (7)

0.31 g (0.5 mmol) [(Et$_2$O)Na]Cr$_2$Me$_8$ was dissolved in 20 mL diethyl ether and cooled to -30 °C. The addition of 0.38 mL (2 mmol) TMCDA produced a red brown solution which was stirred for 1 h. After concentration *in vacuo* the solution was stored at -30 °C giving yellow green crystals in a 38 % (0.15 g) yield. ^{1}H NMR (400.13 MHz, C_6D_6, 300 K: δ(ppm) = 2.29 (bs, 36 H, C*H*$_3$ TMCDA), 2.12 (bs, 6 H, C*H* TMCDA), 1.51 (bs, 12 H, C*H*$_2$ TMCDA), 0.80 (bs, 12 H, C*H*$_2$ TMCDA). ^{13}C{^{1}H} NMR (100.62 MHz, C_6D_6, 300 K): δ(ppm) = 63.7 (*C*H$_3$ TMCDA), 40.8 (*C*H TMCDA), 25.4 (*C*H$_2$ TMCDA), 22.5 (*C*H$_2$ TMCDA).

Acknowledgements

REM thanks the Royal Society for a Wolfson Merit Award and SS thanks the Royal Society of Chemistry for a J W T Jones Travelling Fellowship grant. We also thank Dr. Lewis Maddock for help with some experimental aspects.

References

1. S. P. Green, C. Jones and A. Stasch, *Science*, 2007, **318**, 1754-1757.
2. I. Resa, E. Carmona, E. Gutierrez-Puebla and A. Monge, *Science*, 2004, **305**, 1136-1138.
3. T. Nguyen, A. D. Sutton, M. Brynda, J. C. Fettinger, G. J. Long and P. P. Power, *Science*, 2005, **310**, 844-847.
4. a) K. A. Kreisel, G. P. A. Yap, O. Dmitrenko, C. R. Landis and K. H. Theopold, *J. Am. Chem. Soc.*, 2007, **129**, 14162-14163; b) A. Noor, F. R.

Wagner and R. Kempe, *Angew. Chem. Int. Ed.*, 2008, **47**, 7246-7249; c) Y.-C. Tsai, C.-W. Hsu, J.-S. K. Yu, G.-H. Lee, Y. Wang and T.-S. Kuo, *Angew. Chem. Int. Ed.*, 2008, **47**, 7250-7253; d) A. Noor, G. Glatz, R. Müller, M. Kaupp, S. Demeshko and R. Kempe, *Nature Chem.*, 2009, **1**, 322-325; e) C.-W. Hsu, J.-S. K. Yu, C.-H. Yen, G.-H. Lee, Y. Wang and Y.-C. Tsai, *Angew. Chem. Int. Ed.*, 2009, **47**, 9933-9936.

5. a) D. L. Lichtenberger, M. A. Lynn and M. H. Chisholm, *J. Am. Chem. Soc.*, 1999, **121**, 12167-12176; b) G. La Macchia, L. Gagliardi, P. P. Power and M. Brynda, *J. Am. Chem. Soc.*, 2008, **130**, 5104-5114; c) C. Ni, B. D. Ellis, G. J. Long and P. P. Power, *Chem. Commun.*, 2009, 2332-2334; d) M. Carrasco, M. Faust, R. Peloso, A. Rodriguez, J. Lopez-Serrano, E. Alvarez, C. Maya, P. P. Power and E. Carmona, *Chem. Commun.*, 2012, **48**, 3954-3956; e) S. E. Brown-Xu, M. H. Chisholm, C. B. Durr and T. F. Spilker, *J. Am. Chem. Soc.*, 2013, **135**, 8254-8259; f) S. E. Brown-Xu, M. H. Chisholm, C. B. Durr, S. A. Lewis, T. F. Spilker and P. J. Young, *Chem. Sci.*, 2014, **5**, 2657-2666; g) M. Carrasco, I. Mendoza, M. Faust, J. Lopez-Serrano, R. Peloso, A. Rodriguez, E. Alvarez, C. Maya, P. P. Power and E. Carmona, *J. Am. Chem. Soc.*, 2014, **136**, 9173-9180; h) M. H. Chisholm, S. E. Brown-Xu and T. F. Spilker, *Acc. Chem. Res.*, 2015, **48**, 877-885.
6. a) H. Breil and G. Wilke, *Angew. Chem. Int. Ed.*, 1966, **5**, 898-899; b) D. J. Brauer and C. Krüger, *Inorg. Chem.*, 1976, **15**, 2511-2514; c) F. A. Cotton, S. A. Koch, A. J. Schultz and J. M. Williams, *Inorg. Chem.*, 1978, **17**, 2093-2098.
7. a) J. Krausse, G. Marx and G. Schödl, *J. Organomet. Chem.*, 1970, **21**, 159-168; b) F. A. Cotton, J. M. Troup, T. R. Webb, D. H. Williamson and G. Wilkinson, *J. Am. Chem. Soc.*, 1974, **96**, 3824-3828; c) F. A. Cotton, S. A. Koch, K. Mertis, M. Millar and G. Wilkinson, *J. Am. Chem. Soc.*, 1977, **99**, 4989-4992; d) D. M. Collins, F. A. Cotton, S. A. Koch, M. Millar and C. A. Murillo, *Inorg. Chem.*, 1978, **17**, 2017-2020.
8. a) R. E. Mulvey, *Organometallics*, 2006, **25**, 1060-1075; b) D. R. Armstrong, W. Clegg, S. H. Dale, D. V. Graham, E. Hevia, L. M. Hogg, G. W. Honeyman, A. R. Kennedy and R. E. Mulvey, *Chem. Commun.*, 2007, 598-600; c) S. Merkel, D. Stern, J. Henn and D. Stalke, *Angew. Chem. Int. Ed.*, 2009, **48**, 6350-6353; d) P. Garcia-Alvarez, R. E. Mulvey and J. A. Parkinson, *Angew. Chem. Int. Ed.*, 2011, **50**, 9668-9671; e) B. Haag, M. Mosrin, H. Ila, V. Malakhov and P. Knochel, *Angew. Chem. Int. Ed.*, 2011, **50**, 9794-9824; f) F. Mongin and A. Harrison-Marchand, *Chem. Rev.*, 2013, **113**, 7563-7727.
9. a) J. J. H. Edema and S. Gambarotta, *Comments Inorg. Chem.*, 1991, **11**, 195-214; b) S. Hao, S. Gambarotta and C. Bensimon, *J. Am. Chem. Soc.*, 1992, **114**, 3557-3559; c) S. Hao, J.-I. Song, P. Berno and S. Gambarotta, *Organometallics*, 1994, **13**, 1326-1335.
10. a) E. Weiss, *Angew. Chem. Int. Ed.*, 1993, **32**, 1501-1503; b) D. V. Graham, E. Hevia, A. R. Kennedy and R. E. Mulvey, *Organometallics*, 2006, **25**, 3297-3300; c) J. A. Garden, A. R. Kennedy, R. E. Mulvey and S. D. Robertson, *Dalton Trans.*, 2011, **40**, 11945-11954; d) S. E. Baillie, W. Clegg, P. Garcia-Alvarez, E. Hevia, A. R. Kennedy, J. Klett and L. Russo, *Organometallics*, 2012, **31**, 5131-5142; e) R. E. Mulvey and S. D. Robertson, *Top. Organomet. Chem.*, 2013, **45**, 103-140.
11. R. Campbell, L. M. Carrella, W. Clegg, R. E. Mulvey, E. Rentschler, S. D. Robertson and L. Russo, *Inorg. Chem.*, 2011, **50**, 4656-4659.

12. C. Ni and P. P. Power, *Organometallics*, 2009, **28**, 6541-6545.
13. a) T. Susuki and J. Tsuji, *J. Org. Chem.*, 1970, **35**, 2982-2986; b) R. C. Kerber and B. R. Waldbaum, *J. Organomet. Chem.*, 1996, **513**, 277-280; c) H. Tsurugi, K. Yamada, M. Majumdar, Y. Sugino, A. Hayakawa and K. Mashima, *Dalton Trans.*, 2011, **40**, 9358-9361; d) P. W. Jolly, *Acc. Chem. Res.*, 1996, **29**, 544-551; e) H. Tsurugi, A. Hayakawa, S. Kando, Y. Sugino and K. Mashima, *Chem. Sci.*, 2015, **6**, 3434-3439.
14. a) A. Bollmann, K. Blann, J. T. Dixon, F. M. Hess, E. Killian, H. Maumela, D. S. McGuinness, D. H. Morgan, A. Neveling, S. Otto, M. Overett, A. M. Z. Slawin, P. Wassersheid and S. Kuhlmann, *J. Am. Chem. Soc.*, 2004, **126**, 14712-14713; b) S. Peitz, B. R. Aluri, N. Peulecke, B. H. Müller, A. Wöhl, W. Müller, M. H. Al-Hamzi, F. M. Mosa and U. Rosenthal, *Chem. Eur. J.*, 2010, **16**, 7670-7676; c) S. Licciulli, I. Thapa, K. Albahily, I. Korobkov, S. Gambarotta, R. Duchateau, R. Chevalier and K. Schuhen, *Angew. Chem. Int. Ed.*, 2010, **49**, 9225-9228; d) P. R. Elowe, C. McCann, P. G. Pringle, S. K. Spitzmesser and J. E. Bercaw, *Organometallics*, 2006, **25**, 5255-5260; e) Y. Shaikh, J. Gurnham, K. Albahily, S. Gambarotta and I. Korobkov, *Organometallics*, 2012, **31**, 7427-7433; f) Y. Shaikh, K. Albahily, M. Sutcliffe, V. Fomitcheva, S. Gambarotta, I. Korobkov and R. Duchateau, *Angew. Chem. Int. Ed.*, 2012, **51**, 1366-1369.
15. F. A. Cotton, C. A. Murillo and R. A. Walton, *Multiple Bonds between Metal Atoms*, Springer, New York, 2005.
16. a) T. Soda, Y. Kitagawa, T. Onishi, Y. Takano, Y. Shigeta, H. Nagao, Y. Yoshioka and K. Yamaguchi, *Chem. Phys. Lett.*, 2000, **319**, 223-230; b) K. Yamaguchi, Y. Takahara and T. Fueno, in *Applied Quantum Chemistry*, ed. V. H. Smith, Riedel, Dordrecht, The Netherlands, 1986, p. 155.
17. F. A. Cotton, L. M. Daniels, E. A. Hillard and C. A. Murillo, *Inorg. Chem.*, 2002, **41**, 2466-2470.
18. a) J. F. Berry, E. Bothe, F. A. Cotton, S. A. Ibragimov, C. A. Murillo, D. Villagran and X. Wang, *Inorg. Chem.*, 2006, **45**, 4396-4406; b) D. W. Brogden, Y. Turov, M. Nippe, G. Li Manni, E. A. Hillard, R. Clerac, L. Gagliardi and J. F. Berry, *Inorg. Chem.*, 2014, **53**, 4777-4790.
19. F. Neese, *J. Phys. Chem. Solids*, 2004, **65**, 781-785.
20. a) L. M. Wilson and R. D. Cannon, *Inorg. Chem.*, 1988, **27**, 2382-2383; b) N. M. Alfaro, F. A. Cotton, L. M. Daniels and C. A. Murillo, *Inorg. Chem.*, 1992, **31**, 2718-2723; c) O. M. El-Kadri, M. J. Heeg and C. H. Winter, *Inorg. Chem.*, 2006, **45**, 5278-5280; d) A. R. Sadique, M. J. Heeg and C. H. Winter, *J. Am. Chem. Soc.*, 2003, **125**, 7774-7775.
21. a) M. Brynda, L. Gagliardi, P.-O. Widmark, P. P. Power and B. O. Roos, *Angew. Chem. Int. Ed.*, 2006, **45**, 3804-3807; b) M. Brynda, L. Gagliardi and B. O. Roos, *Chem. Phys. Lett.*, 2009, **471**, 1-10; c) G. Li Manni, A. L. Dzubak, A. Mulla, D. W. Brogden and J. F. Berry, *Chem. Eur. J.*, 2012, **18**, 1737-1749.
22. G. M. Sheldrick, *Acta Crystallogr.*, 2007, **A64**, 112-122.
23. O. V. Dolomanov, L. J. Bourhis, R. J. Gildea, J. A. K. Howard and H. Puschmann, *J. Appl. Cryst.*, 2009, **42**, 339-341.
24. F. Neese, *WIREs Comput. Mol. Sci.*, 2012, **2**, 73-78.
25. a) J. P. Perdew, *Phys. Rev. B.*, 1986, **33**, 8822-8824; b) A. D. Becke, *Phys. Rev. A.*, 1988, **38**, 3098-3100.
26. a) R. Ahlrichs and K. May, *Phys. Chem. Chem. Phys.*, 2000, **2**, 943-945; b) F. Weigend and R. Ahlrichs, *Phys. Chem. Chem. Phys.*, 2005, **7**, 3297-3305.

27. a) J. P. Perdew, K. Burke and M. Ernzerhof, *Phys. Rev. Lett.*, 1996, **77**, 3865-3868; b) J. P. Perdew, K. Burke and M. Ernzerhof, *Phys. Rev. Lett.*, 1997, **78**, 1396; c) C. Adamo and V. Barone, *J. Chem. Phys.*, 1999, **110**, 6158-6170.
28. a) E. van Lenthe, J. G. Snijders and E. J. Baerends, *J. Chem. Phys.*, 1996, **105**, 6505-6516; b) E. van Lenthe, A. van der Avoird and P. E. S. Wormer, *J. Chem. Phys.*, 1998, **108**, 4783-4796; c) E. van Lenthe, S. Faas and J. G. Snijders, *Chem. Phys. Lett.*, 2000, **328**, 107-112.
29. S. Grimme, J. Antony, S. Ehlrich and H. Krieg, *J. Chem. Phys.*, 2010, **132**, 154104.
30. F. Neese, F. Wennmohs, A. Hansen and U. Becker, *Chem. Phys.*, 2009, **356**, 98-109.
31. a) K. Eichkorn, O. Treutler, H. Öhm, M. Haser and R. Ahlrichs, *Chem. Phys. Lett.*, 1995, **242**, 652-660; b) K. Eichkorn, F. Weigend, O. Treutler and R. Ahlrichs, *Theor. Chem. Acc.*, 1997, **97**, 119-124.
32. A. Klamt and G. Schüürmann, *J. Chem. Soc., Perkin Trans.*, 1993, **2**, 799-805.
33. a) P. Pulay, *Chem. Phys. Lett.*, 1980, **73**, 393-398; b) P. Pulay, *J. Comput. Chem.*, 1982, **3**, 556-560.
34. a) L. Noodleman, *J. Chem. Phys.*, 1981, **74**; b) L. Noodleman, D. A. Case and A. Aizman, *J. Am. Chem. Soc.*, 1988, **110**, 1001-1005; c) L. Noodleman and E. R. Davidson, *Chem. Phys.*, 1986, **109**, 131-143; d) L. Noodleman, J. G. Norman Jr., J. H. Osborne, A. Aizman and D. A. Case, *J. Am. Chem. Soc.*, 1985, **107**, 3418-3426; e) L. Noodleman, C. Y. Peng, D. A. Case and J.-M. Monesca, *Coord. Chem. Rev.*, 1995, **144**, 199-244.
35. Molekel, Advanced Interactive 3D-Graphics for Molecular Sciences, Swiss National Supercomputing Centre. http://www.cscs.ch/molekel).